

A model for the spatial distribution of relativistic electrons in the Crab Nebula

E. Amato¹, M. Salvati², R. Bandiera², F. Pacini^{1,2}, L. Woltjer^{2,3}

¹ Dipartimento di Astronomia e Scienza dello Spazio, Università di Firenze, Largo E. Fermi 5, I-50125 Firenze, Italy

² Osservatorio Astrofisico di Arcetri, Largo E. Fermi 5, I-50125 Firenze, Italy

³ Observatoire de Haute-Provence, F-04870 Saint Michel l'Observatoire, France

Abstract. We extend the homogeneous model for the synchrotron emission from plerions to allow more realistic predictions of the surface brightness profiles of the Crab Nebula at radio, optical and X-ray frequencies. Abandoning the assumption of a uniform particle distribution, we assume that particles are injected into the synchrotron nebula only in the vicinity of the pulsar. Their distribution is then determined, to zeroth order, by MHD propagation in an azimuthal magnetic field of spatially constant but time-dependent intensity. A good agreement with observations across the electromagnetic spectrum is obtained if the finite extension of the particle injection region and particle diffusion with respect to the azimuthal field lines are taken into account.

Key words: ISM: supernova remnants - ISM: individual objects: Crab Nebula - Radiation mechanisms: non-thermal

1. Introduction

The synchrotron spectrum of the Crab Nebula, the prototype of the plerion class, is described, from the radio to the soft X-ray band, by the succession of three power laws ($S_\nu \propto \nu^{-\alpha}$) of increasing index. The present best estimates of the power indices are: $\alpha_R = 0.27 \pm 0.04$ for frequencies ranging from 100 MHz to 1.2×10^{13} Hz (Bietenholz et al. 1997 based on Kovalenko et al. 1994), $\alpha_O \simeq 0.7 \pm 0.1$ for $10^{13} \text{ Hz} < \nu < 10^{15} \text{ Hz}$ (Véron-Cetty & Woltjer 1993), and $\alpha_X = 1.14$ for photon energies below 50 keV (Véron-Cetty & Woltjer 1993 based on Toor & Seward 1974).

This non-thermal spectrum is well accounted for within the framework of the homogeneous model by Pacini & Salvati (1973, hereafter PS), who regard the plerion as an adiabatically expanding spherical bubble of magnetized relativistic fluid. In their model the bubble is replenished by the continuous conversion of the pulsar's energy outflow into magnetic energy and relativistic particles with a

power-law spectral distribution of index $\gamma = 2\alpha_R + 1$. The energy balance of the plerion is determined by the competition between the decreasing pulsar's input and the losses the fluid undergoes because of radiation and expansion.

When the synchrotron emission of the Crab Nebula is calculated under the assumption of constant expansion rate and uniform spatial distribution of the fluid, both the decline of luminosity with time (Véron-Cetty & Woltjer 1991) and the frequency of the low energy spectral break (Marsden et al. 1984) are correctly predicted, for a magnetic field strength around $3 \times 10^{-4} G$, in agreement with estimates based on equipartition arguments (Woltjer 1958) and also with more recent measurements of the nebular inverse Compton radiation flux (De Jager & Harding 1992).

Despite the success of the model in describing the integrated properties of the Crab Nebula synchrotron emission between radio and optical, the homogeneity assumption prevents any realistic prediction of the luminosity spatial distribution. To cite the main facts: in contrast with what is observed, neither nebular size reduction with increasing observation frequency, nor steepening of the optical radiation spectrum with increasing distance from the central pulsar can be accommodated in the homogeneous scheme.

The assumption of a spatially homogeneous particle distribution is also problematic on physical grounds. High resolution studies of the Crab Nebula show no evidence for particle acceleration sites other than the restricted region within about $30''$ – $60''$ from the central pulsar, in which the optical wisps and the X-ray torus and jets are observed. In view of this, assuming a uniform particle distribution is equivalent to assuming an almost infinite particle diffusion coefficient.

The removal of this assumption is going to be the main modification we shall introduce in the following in the PS model, to allow realistic predictions for the surface brightness profiles of the Crab Nebula from radio to X-ray frequencies.

2. Outline of the model

In our model the nebula is regarded as a sphere of radius $R(t)$, expanding at a constant rate $v \simeq 1.8 \times 10^8 \text{ cm/s}$: $R(t) = R_0 + vt$. A continuous supply of new magnetic energy and particles is provided by the central pulsar, whose energy output per unit time can be written as

$$L(t) = \frac{L_0}{(1 + t/\tau)^\kappa}, \quad (1)$$

where $L_0 \simeq 3 \times 10^{39} \text{ erg/s}$ is the initial pulsar luminosity, and, assuming for the pulsar rotation a constant braking index $n = 2.5$ (Groth 1975), $\tau = 710 \text{ yr}$ is the slowing down time scale of the rotation, and $\kappa = (n + 1)/(n - 1)$.

Both new particles and new magnetic flux are injected into the nebula within a spherical layer at a distance r_0 from the central pulsar. We shall assume that the injection region has, to zeroth order, zero extension, while its location, not known *a priori*, has to be determined by comparison between the model predictions for surface brightness profiles and the data.

We assume that the particles' velocity distribution is isotropic and that each particle emits essentially at its characteristic frequency: $\nu_c = c_2 B_\perp E^2$, where $c_2 = 0.29 \times (3ec/4\pi(mc^2)^3)$ is a constant, $B_\perp = B \sin\theta$, and E and θ are the particle's energy and pitch angle respectively. Under these assumptions the nebular synchrotron emissivity becomes

$$S_\nu(\nu, t, r) = \frac{c_1}{2c_2} \int_\Omega \frac{d\Omega}{4\pi} \left(\frac{B_\perp \nu}{c_2} \right)^{\frac{1}{2}} N \left[\left(\frac{\nu}{c_2 B_\perp} \right)^{\frac{1}{2}}, t, r \right], \quad (2)$$

with $c_1 = (2c/3)(e/mc^2)^4$ being a constant and $N(E, t, r)$ representing the particles' spectral and spatial density at time t . The integral represents the average over particles' pitch angles.

As in PS we regard the magnetic field as spatially constant, therefore, in our model, both the spatial and spectral characteristics of the nebular synchrotron emission are directly related to the particle spatial and spectral distribution, $N(E, t, r)$.

$N(E, t, r)$ is related to the injected particles' spectrum by the particles' number conservation law:

$$N(E, t, r) = \frac{J[E_i(E, t, r), t_i(E, t, r)] \left| \frac{\partial t_i \partial E_i}{\partial r \partial E} \right|}{4\pi r^2}, \quad (3)$$

with J being the number of newly injected particles per unit time and energy interval and E_i and t_i being, respectively, the initial energy and injection time of a given particle. The last term in Eq. 3 represents the jacobian of the transformation $(t_i, E_i) \rightarrow (r, E)$.

Apart from knowledge of the injected spectrum, in order to calculate $N(E, t, r)$ from this equation, knowledge of the particles' age $(t - t_i)$ and initial energy (E_i) as functions of their present position (r) and energy (E) is needed.

We consider the energy evolution of each particle due to adiabatic and synchrotron losses:

$$\frac{dE}{dt} = -\frac{E}{3} \nabla \cdot \mathbf{u} - c_1 B_\perp^2 E^2. \quad (4)$$

Once the magnetic field \mathbf{B} and the fluid bulk velocity \mathbf{u} are known at each time, Eq. 4 can be integrated to determine $E_i(E, r)$.

The determination of the time dependence of the magnetic field strength B is straightforward under our assumptions of time constancy of the nebular expansion rate and spatial constancy of B itself. Following PS, we relate B to the nebular content of magnetic energy $W_B(t)$: $B^2(t) = 8\pi W_B(t)/V(t)$, with $V(t) = (4\pi/3)(R^3(t) - r_0^3)$ representing the confining volume for the magnetic field. Then we write the time evolution of W_B due to expansion losses and the decreasing pulsar input:

$$\frac{dW_B}{dt} = -\frac{W_B}{3} \frac{d}{dt} \ln V(t) + \beta L(t). \quad (5)$$

Integration of Eq. 5, where β is a constant, yields the magnetic field strength at each time as a function of its present average value, which we take to be around $3 \times 10^{-4} \text{ G}$.

Knowing $B(t)$, and further assuming that the magnetic field is azimuthal, $\mathbf{B} = B(t)\mathbf{e}_\phi$, we can use the flux freezing condition,

$$\frac{\partial \mathbf{B}}{\partial t} = \nabla \wedge (\mathbf{u} \wedge \mathbf{B}), \quad (6)$$

as an equation for the fluid bulk velocity \mathbf{u} , which we assume to be radial: $\mathbf{u} = u(r, t)\mathbf{e}_r$. Integrating Eq. 6 with the boundary condition that the fluid velocity field matches the expansion velocity of the nebula at its outer edge ($u(R(t), t) = v$), we find:

$$u(r, t) = \frac{vR(t)}{r} + \frac{\partial \ln B}{\partial t} \frac{(R^2(t) - r^2)}{2r}. \quad (7)$$

Eq. 7 can also be written as

$$\frac{d}{dt} [B(t)(R^2(t) - r^2(t))] = 0, \quad (8)$$

which yields, in its integral form:

$$B(t)(r^2 - r_0^2) = B(t_i)(R^2(t) - r_0^2) - B(t_i)(R^2(t_i) - r_0^2). \quad (9)$$

This last equation simply states that the magnetic flux injected into the nebula during the time interval $t - t_i$, with t_i being the time at which a particle that at time t is at r was born, is all contained between r_0 and r . Taking $r = r(t, t_i)$ from Eq. 9, we have got the relation needed to connect the particles' position at each time to their age.

Our assumptions for the magnetic field structure deserve a few comments. First of all, we notice that from the point of view of dynamics, assuming a spatially constant intensity of the magnetic field is physically equivalent to

state that the magnetic contribution to the total pressure is dominant through the entire nebula. Secondly, concerning the assumption of an azimuthal field orientation theoretical expectations and polarization studies at radio and optical wavelengths (Wilson 1972a, Woltjer 1958) suggest that this should be a good approximation at least in the inner part of the nebula. Nevertheless the percentage of polarization observed (around 30% and 10%, on average, at optical and radio frequencies, respectively), although high, is still less than what one would expect if the field were perfectly ordered. Moreover, toward the edges of the nebula there seems to be evidence, on the polarization maps, of the magnetic field structure becoming predominantly radial. These facts are ignored in this section but in the following we shall try to take them into account, at least in a perturbative manner.

Presently what is left to determine, before being able to calculate $N(E, t, r)$ as a function of the injected spectrum, is the evolution of the particles' energy from initial to present value. Introducing the expression found for \mathbf{u} into Eq. 4, we obtain:

$$\frac{d}{dt} \left[\frac{1}{E} \left(\frac{B(t)}{r} \right)^{1/3} \right] = c_1 \frac{B(t)^{7/3}}{r^{1/3}} \sin^2 \theta. \quad (10)$$

We integrate Eq. 10 after replacing $\sin^2 \theta$ with its time-average. We take this to be $2/3$, which is equivalent to state that each particle during its synchrotron lifetime experiences all the possible velocity orientations with respect to the magnetic field with the same probability. Obviously, we expect this approximation to work better the longer a particle lives, hence the smaller its initial energy is. Nevertheless we apply it to particles of all energies and finally find the expression for $E_i(E, t, r)$:

$$E_i(E, t, r) = E \left(\frac{r}{r_0} \right)^{1/3} \left(\frac{B(t_i)}{B(t)} \right)^{1/3} \left(1 - \frac{E}{E_b(t, r)} \right)^{-1} \quad (11)$$

with

$$E_b(t, r) = \frac{3}{2c_1} \left(\frac{B(t)}{r} \right)^{1/3} \left(\int_{t_i(r)}^t \frac{B(t')^{7/3}}{r(t')^{1/3}} dt' \right)^{-1}. \quad (12)$$

The meaning of the energy $E_b(t, r)$ is apparent: it represents the maximum possible energy for particles that at time t reside at r . Substituting E_b with $\sqrt{\nu/(c_2 B_\perp)}$, Eq. 11 also defines the maximum radial distance $r_M(\nu, t)$ from which we expect emission to come for a given frequency. Hence it can be used to describe the decrease of nebular size with increasing observation frequency.

Inserting our findings into Eq. 3 we are finally able to relate $N(E, t, r)$ to the injected particle spectrum.

Concerning the latter some assumption is necessary. Assuming that the injected electron spectrum is described by a single power-law, synchrotron aging can account for just one break in the emission spectrum, while observations show that there are at least two. Therefore there

must be an intrinsic break in the injected electron spectrum. We take it to be:

$$J(E, t) = \begin{cases} K_1(t) E^{-\gamma_1} ; & E_m < E < E_1 \\ K_2(t) E^{-\gamma_2} ; & E_1 < E < E_M \\ 0 ; & E < E_m \text{ or } E > E_M . \end{cases} \quad (13)$$

As to the location of the intrinsic break E_1 and the values of the power indices, we follow PS and take a common injection law for radio and optical emitting particles, that is $\gamma_1 = 2\alpha_R + 1 = 2\alpha_O = 1.54$, $\gamma_2 = 2\alpha_X = 2.3$ and E_1 in the range of UV emitting particles.

For simplicity, we assume all the energy cuts to be time independent and the ratio between K_1 and K_2 to remain constant. If we then consider that a constant fraction β of the pulsar's energy outflow goes into feeding the magnetic field, with the remaining $1 - \beta$ being used for accelerating particles, the constraint on the total slowing-down power converted into particles,

$$(1 - \beta)L(t) = \int_{E_m}^{E_M} J(E, t) E dE, \quad (14)$$

implies

$$K_1(t) \propto K_2(t) \propto L(t). \quad (15)$$

Finally we have for the spectral and spatial distribution of particles across the nebula:

$$N(E, t, r) = \frac{\bar{N}}{(1 + t_i(r)/\tau)^\kappa} E^{-\gamma} \left(\frac{r_0 B(t)}{r B(t_i(r))} \right)^{\frac{\gamma-1}{3}} \times \left[1 - \frac{E}{E_b(t, r)} \right]^{\gamma-2} \frac{1}{4\pi r^2} \frac{\partial t_i}{\partial r}, \quad (16)$$

with

$$\gamma = \begin{cases} \gamma_1, & E_m(r) < E < E_1(r) \\ \gamma_2, & E_1(r) < E < E_M(r) \end{cases} \quad (17)$$

where the energies $E_m(r)$, $E_M(r)$ and $E_1(r)$ are the evolved minimum, maximum and intrinsic break energy at radius r , respectively, and can be calculated as functions of E_m , E_M and E_1 by use of Eq. 11.

3. Comparison with the data

Within the frame of our assumptions, the only unknowns in Eq. 16 are the injection radius r_0 , the magnetic field strength B , which is only known with some uncertainty, and \bar{N} , the last containing the cut off energies of the injected spectrum. These parameters have very different observational signatures: the first one is related to the radial distance from the central pulsar of the luminosity peak, the second mostly affects the nebular extension at different frequencies (as it is apparent from Eq. 11) and the third one only affects the overall nebular synchrotron flux.

To determine the best-fit values of our parameters, the model predictions for the synchrotron surface brightness

profile of the Crab Nebula have been compared with high resolution data at various frequencies.

For the radio band we have used a VLA map at a frequency of 1.4 GHz (Bietenholz et al. 1997).

The spatial and spectral distribution of the optical synchrotron continuum was determined by Véron-Cetty & Woltjer (1993) after subtraction of the thermal contributions from foreground stars and filaments, from four narrow-band images at wavelengths of 9241, 6450, 5364 and 3808 Å. We have reanalysed these maps, kindly put at our disposal by M.P. Véron-Cetty, with sophisticated star subtraction algorithms.

Finally, in the X-ray band, we have used, after deconvolution of the instrumental PSF and subtraction of the dust halo (Bandiera et al. 1998), a collection of all the public ROSAT HRI data concerning the Crab Nebula. We have estimated the mean photon energy of these data to be 1 keV.

Within the frame of this model (zeroth order model hereafter), the synchrotron surface brightness J_ν is simply obtained by integration of Eq. 2 along the line of sight:

$$J_\nu(\nu, t, z) = \int_z^{R(t)} S_\nu(\nu, t, r) \frac{r dr}{\sqrt{r^2 - z^2}}, \quad (18)$$

with the expression for the particle number density N in S_ν calculated from Eq. 16.

In order to compare our spherical model with the observations, we have extracted from each image what we call a “radial intensity profile”: we first sampled the emission profiles of the nebula along different directions, taking the mean values over small areas of $10'' \times 10''$ and then, after rescaling the different axes to a common length, we averaged those profiles. The procedure just described, to which we refer in the following as “data sphericization”, is the main cause of uncertainty in our radial profiles and it is what we take into account in the error bars attached to the data points in most of the following plots.

Since for any value of B below 5×10^{-3} G the evolution of radio emitting particles is essentially adiabatic (which translates into $E/E_b(t, r)$ in Eq. 16 approaching unity only toward the very outer edge of the nebula), at these frequencies the magnetic field strength simply results in a multiplying factor in the expression of J_ν and does not much affect the shape of the emission profile. This fact allowed us to determine r_0 and the product $\bar{N} B^{(1+\gamma)/2}$ (see Eqs. 2 and 16) by fitting the radio data alone. Our best fit estimate gave $r_0 = 10''$, which, for a 2 kpc distance to the Crab Nebula, translates into $r_0 = 0.1$ pc.

Our best fit radial profile at 1.4 GHz is plotted against the data in Fig.1. Our best fit value of r_0 yields a distance from the pulsar of the injection site fully compatible with the association between the particle acceleration region and the location of the optical wisps.

However, given this value of r_0 and a magnetic field intensity around 3×10^{-4} G, so as to reproduce the observed ratio between radio and optical fluxes for an assumed value

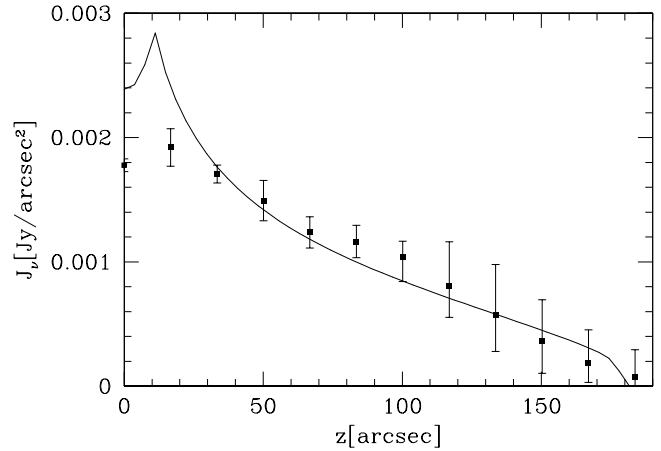


Fig. 1. Comparison with the data (points) at 1.4 GHz of our zeroth order prediction of the surface brightness profile (solid curve) for $r_0 = 10''$. The error bars attached to the data points take account of the uncertainties introduced by “data sphericization”, with the upper and lower limits following the emission profiles along the major and minor axis, respectively.

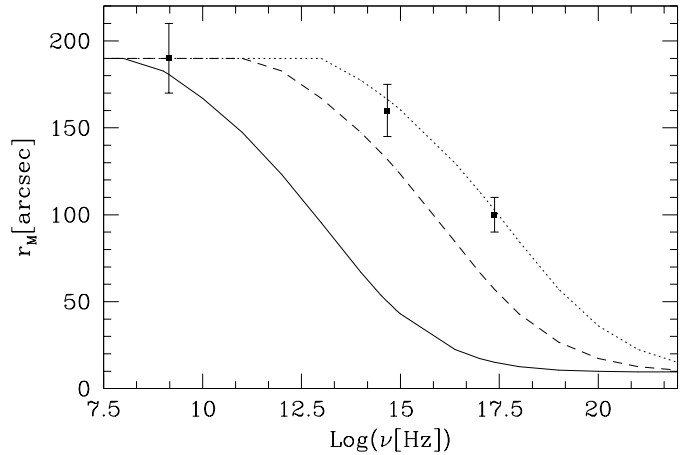


Fig. 2. Our zeroth order model expectations for the dependence of nebular size on frequency. The extension of the nebula (defined as the outermost radius from which photons of a given frequency are emitted according to Eq. 11) as a function of frequency is shown for $r_0 = 0.1$ pc and three different values of the present average magnetic field: $B = 3 \times 10^{-4}$ G (solid curve), $B = 3 \times 10^{-5}$ G (dashed curve) and $B = 10^{-5}$ G (dotted curve). The points represent the extension (1 % intensity radius) of the nebula at radio, optical and X-ray frequencies, as given by our images. The upper and lower limits on the first two points represent the measurements along the major and minor axis, respectively, while the X-ray nebula is larger along the direction of the radio and optical minor axis.

of the interstellar absorption $A_v = 1^m.5$ (Véron-Cetty & Woltjer 1993), the nebular size at optical and X-ray frequencies is largely underestimated.

In Fig.2 we plot, versus observation frequency, $r_M(\nu)$, defined by Eq. 11 as the outermost radius from which photons of a given energy can be emitted. It is apparent from

that figure that the extension of the nebula at optical and X-ray frequencies may only be reproduced by assuming a magnetic field strength $B \simeq 10^{-5}$ G.

Such a low value of B is easily proved to be incompatible with a series of observational constraints and in any case is inconsistent with our assumption of a magnetically dominated flow, which holds only for values of the magnetic field strength above the equipartition requirement: with a field as low as 10^{-5} G the particle pressure would be dominant and the assumption of a constant magnetic field invalid.

4. Particle diffusion

The discrepancies between the model expectations and the high frequency observations induced us to take into account the possibility that particles diffuse with respect to the azimuthal magnetic field lines.

We have taken this fact into account in a perturbative manner, convolving our zeroth order predicted particle distribution, given by Eq. 16 and hereafter referred to as $N_0(E, t, r)$, with a gaussian G of energy dependent width σ :

$$N(E, t, r) = \int_{\Omega} \int_{r_0}^{R(t)} N_0(E, t, r') G(\mathbf{r} - \mathbf{r}', t, E) dr', \quad (19)$$

with

$$\sigma^2(E, t, r') = D_a + D_0 \int_{t_i(r')}^t \tilde{E}^\alpha(t', r', E) dt'. \quad (20)$$

where D_0 and D_a are constants, and \tilde{E} represents the energy at time t' assigned by our zeroth order model to a particle which at time t is found at r' with energy E .

Our choice of the functional form of σ was guided by the following consideration. We expected the smearing of the particles' distribution to increase with increasing disorder of the magnetic field structure and with increasing possibility for the particles to jump from one magnetic flux tube to the other, both of which effects make our MHD transport hypothesis an increasingly poor approximation.

In view of this, first of all, the gaussian width had to increase with increasing distance from the central pulsar, since, as already mentioned, toward the outer edges of the nebula we know from polarization studies that the magnetic field structure becomes more and more distorted. Secondly, σ also had to increase with increasing particle Larmor radii. This accounts for the assumed form of the second term in the expression of σ^2 , which in fact grows both with elapsed time and with history-averaged particle energy. The first term, the only remaining for $r' = r_0$, is a measure of the radial extent of the particle injection region. As to the first one, since the term just discussed vanishes for $r' = r_0$, the interpretation of D_a as the squared radius of the particle injection region is straightforward.

We have determined α , D_0 and D_a by a multifrequency fit to the data. For a magnetic field intensity of 3.5×10^{-4}

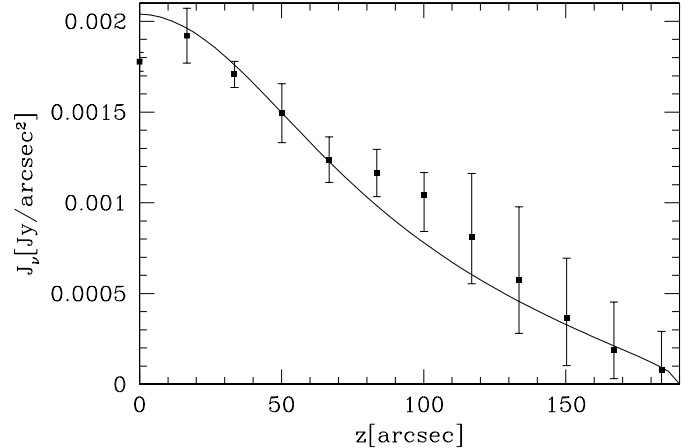


Fig. 3. Comparison between the model (solid curve) and the radio data (points) at 1.4 GHz for the best fit values of the parameters.

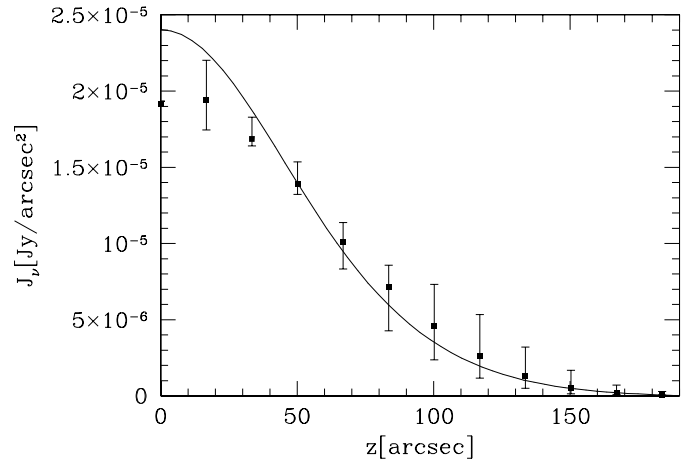


Fig. 4. Comparison between the model and the optical data at 6450 Å for the best fit values of the parameters.

G and an injection radius of $10''$ we have found $\alpha = 0.2$ and $D_a = (48'')^2$.

The figures from 3 to 5 show our best fit radial profiles at radio, optical and X-ray frequencies plotted against the data. Our predicted profiles are outside the error bars of the data only in the inner part of the nebula, where our assumptions are definitely too simplified. The only other discrepancy is found in the radio emissivity profile (Fig. 3), but the enhancement of the radio emission at a radial distance of around $100''$ is due to the emission of the thermal filaments which our model cannot account for.

Concerning the best fit values of the parameters in σ , a couple of things are worth noticing. First of all, we point out that our best fit estimate for the parameter D_a is in agreement with the size ($30''$ – $60''$) of the central region of the nebula (delineated, as already mentioned, by the X-ray torus), to which particles' acceleration is generally believed to be confined. The best fit value of D_a has a strong dependence on the chosen value of the magnetic

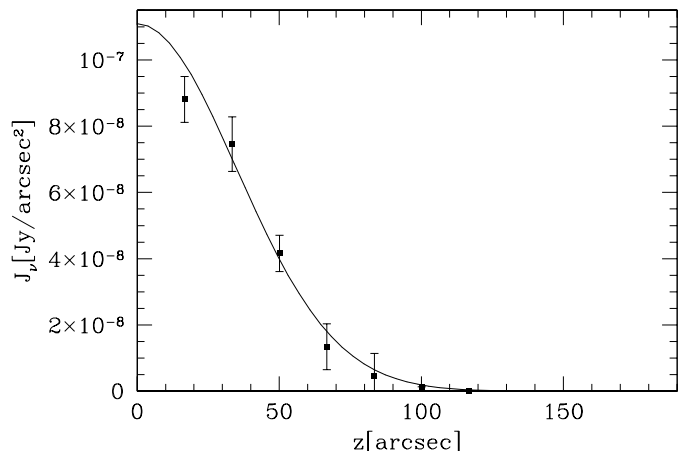


Fig. 5. Comparison between the model and the soft X-ray data at a mean photon energy of 1 keV for the best fit values of the parameters.

field, as long as radio and optical data only are considered, but it is very well fixed (and then can be used to constrain the magnetic field strength), as soon as the X-ray nebula is taken into account.

Secondly, although we end up with a very mild dependence on energy of the gaussian width, this dependence cannot be eliminated. The value of the coefficient α is very well determined by our fit (with an uncertainty of order 10%) and it is also quite insensitive to changes in the assumed magnetic field strength or in the value of r_0 .

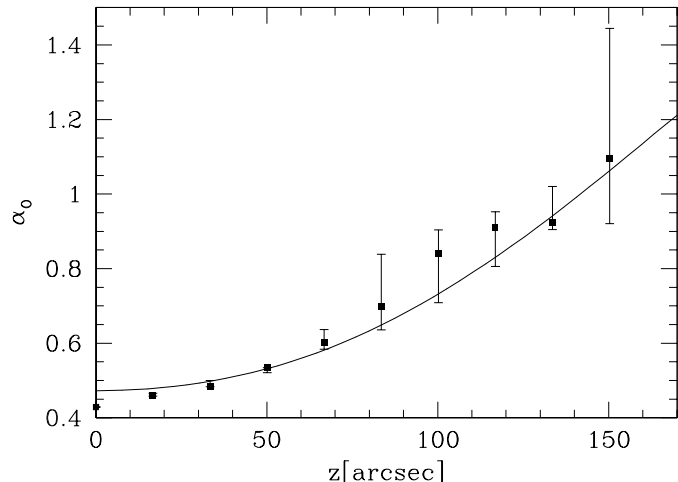


Fig. 6. The predicted spatial variation of optical spectral index between 9241 and 5364 Å plotted against the data.

Of the four narrow-band optical images available to us, we used just one for fitting purposes, while two others were used for computation of a map of optical spectral index variations across the nebula, to be compared, *a posteriori*, with the expectations of the best fit model. This comparison is shown in Fig.6.

5. Discussion

The model we have developed for the relativistic particle distribution in the Crab Nebula reproduces both the spectral and spatial properties of the nebular synchrotron emission from the radio to the soft X-ray band.

Our starting point was the homogeneous model by Pacini & Salvati (1973) of which we kept most of the assumptions with the exception of particle injection distributed throughout the whole nebula and a disordered structure of the magnetic field. Among the assumptions we have kept the ones that mainly affect the synchrotron emissivity are the form of the injected particle spectrum and the spatial constancy of the magnetic field strength.

Concerning the first one, there is the problem of whether a shock-terminated pulsar wind can produce such a spectrum. The assumption of a power law injection spectrum is common to all models, be they of the PS type or of the MHD flow type of Kennel & Coroniti (1984a,b).

Anyway, the spatial properties of the emission, the explanation of which is the main goal of the present model, are much more affected by the assumptions concerning the magnetic field. The problem of letting the high energy particles travel far enough, which we solved by introducing deviations from MHD transport due to a disordered magnetic field, could also be tackled by introducing a lower magnetic field strength in the inner part of the nebula, as it happens in the case of MHD flows which at the origin are particle dominated (Kennel & Coroniti 1984a). Nevertheless the surface brightness profiles along different directions generally show too gradual a decrease of emissivity going outward to be accounted for within the frame of pure MHD transport.

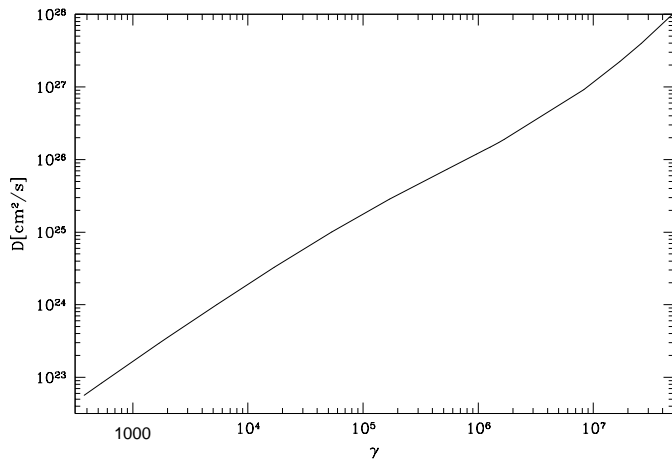
Our model takes into account in a phenomenological manner the effects of deviations of the magnetic field from the very elementary spatial structure assumed at the zeroth order. These have been treated as a perturbation leading to a smearing of the particles' distribution similar to the effects of diffusion.

It is then proper to estimate what diffusion coefficient the model requires. This is done by dividing the spatially averaged best fit σ^2 by the particle synchrotron lifetimes:

$$D \simeq \frac{2}{3} c_1 B^2 \sigma^2 E. \quad (21)$$

We find that D , which we plot in Fig.7 as a function of energy, has approximately the energy dependence appropriate to Bohm's diffusion but our values are about four orders of magnitude higher than what can be obtained in that hypothesis and compatible, for optical particles, with Wilson's estimate (Wilson 1972b): $D \simeq 10^{26} - 10^{27} \text{cm}^2/\text{s}$.

Such high values of the diffusion coefficient are not impossible to obtain as the result of plasma irregularities and offer the interesting possibility of getting from the models information on the detailed magnetic field structure in the nebula.



Wilson A. S., 1972b, MNRAS 160, 355
 Woltjer L., 1958, Bull. Astron. Inst. Neth. 14, 39

Fig. 7. The spatially averaged value of the diffusion coefficient as a function of the particles' Lorentz factor for the best fit values of the model parameters.

There is of course some inconsistency in assuming the magnetic field strength to be spatially constant and the particle distribution to vary, since conditions are rather close to equipartition. We might then expect the magnetic field to be somewhat weaker in the inner parts of the nebula which would improve the fit in the inner parts of Fig. 1. A more detailed modeling of this distribution and of possible instabilities resulting from it is beyond the scope of this paper. Suffice it to note that such instabilities could also contribute to the particle “diffusion”.

We note, however, that the diffusion coefficient obtained through our perturbation approach yields only a very rough estimate, since the perturbing term is of the same order of magnitude as the zeroth order term.

Acknowledgements. This work was partly supported by a grant from ASI. We are indebted to Dr. M.P. Véron-Cetty and Dr. M. F. Bietenholz for putting at our disposal the optical and radio images of the Crab Nebula, respectively.

References

- Bandiera R., Amato E., Woltjer L., 1998, Mem. Soc. Astron. Ital., 69, 901
 Bietenholz M. F., Kassim N., Frail D. A., Perley R. A., Erickson W. C., Hajian A. R., 1997, ApJ 490,291
 De Jager O. C., Harding A. K., 1992, ApJ 396, 161
 Groth E. J., 1975, ApJS 29, 431
 Kennel C. F., Coroniti F. V., 1984a, ApJ 283, 694
 Kennel C. F., Coroniti F. V., 1984b, ApJ 283, 710
 Kovalenko A. V., Pynzar' A. V., Udal'tsov V. A., 1994, Astron. Rep. 38, 110
 Marsden P. L., Gillett F. C., Jennings R. E., Emerson J. P., De Jong T., Olnon F. M., 1984, ApJ 278, L29
 Pacini F., Salvati M., 1973, ApJ 186, 249 (PS)
 Toor A., Seward F. D., 1974, AJ 79, 995
 Véron-Cetty M. P., Woltjer L., 1991, A&A 251, 31
 Véron-Cetty M. P., Woltjer L., 1993, A&A 270, 370
 Wilson A. S., 1972a, MNRAS 157, 229